Front. Struct. Civ. Eng. 2021, 15(1): 244–252
https://doi.org/10.1007/s11709-021-0696-x

RESEARCH ARTICLE

Application of coupled multi-body dynamics–discrete element method for optimization of particle damper for cable vibration attenuation

Danhui DAN[a,b], Qianqing WANG[a*], Jiongxin GONG[a]

[a] *Department of Bridge Engineering, School of Civil Engineering, Tongji University, Shanghai 200092, China*

[b] *College of Civil Engineering and Architecture, Xinjiang University, Urumqi 830047, China*

[*] *Corresponding author. E-mail: wangqq@tongji.edu.cn*

ABSTRACT With the application of the particle damping technology to cable vibration attenuation, the rootless cable damper overcomes the limit in installation height of existing dampers. Damping is achieved through energy dissipation by collisions and friction. In this paper, a coupled multi-body dynamics–discrete element method is proposed to simulate the damping of the damper–cable system under a harmonic excitation. The analyses are done by combining the discrete element method in EDEM and multi-body dynamics in ADAMS. The simulation results demonstrate the damping efficiency of rootless particle damper under different excitations and reveal the influence of the design parameters on its performance, including the filling ratio, particle size, coefficient of restitution, and coefficient of friction.

KEYWORDS granular material, vibration control, discrete element method, particle damper, cable vibration

1 Introduction

The vibration attenuation of stay cable is an essential issue in the cable-stayed bridge design [1]. This flexible and light structure with a low damping can easily vibrate under dynamic loads such as wind, rain, earthquake, and traffic [1,2]. Among the methods used to control the vibration of stay cables, installing a damper is widely present because of its convenient construction and remarkable effect [3]. However, existing dampers, such as oil, sliding surface, and magneto-rheological dampers [3–5], need to be connected to a fixed point, which, in practice, is near the anchorage on the main girder [1]. The maximum damping ratio of a cable with an additional damper is closely related to the installation height of the damper [6]. The limited installation height hinders the damping efficiency of the dampers on the cable.

To overcome this problem, we proposed a rootless cable damper solution, which can be installed at any height of the cable [7]. The use of this damper is an application of the particle damping technology [8] in the field of cable vibration attenuation. It is composed of a cavity cylindrical container fixed to a cable with particles inside the container. Damping is achieved through energy dissipation by collisions and friction among particles and container wall. As there is no limit to the installation height, the damping efficiency of the damper is improved. In this study, we analyze the optimization design of such particle dampers using a novel simulation method.

A damper composed of multiple particles implies a complex and nonlinear damping mechanism owing to numerous factors affecting its damping capabilities and interactions among these factors [8,9]. It is challenging to study its damping performance by theoretical analysis methods. In addition, it is impractical to directly conduct tests. A more feasible method is to use a numerical simulation method for preliminary research [10] for an optimized design.

The discrete element method (DEM) was proposed by Cundall and Strack [11], using contact models to calculate interactions between particles and between particles and structures. This method has been widely used in the research of granular materials in recent years, particularly when a parameter analysis is needed [10,12,13].

Article history: Received Nov 30, 2019; Accepted Apr 5, 2020

As the damping performance of a particle damper depends on the excitation form, it is required to establish a global cable–damper system model for simulations. In this study, a complete cable–damper system was established by coupling the DEM and multi-body dynamics (MBD).

Through the numerical simulation of the cable–damper system, the damping effect of particle dampers on a stay cable is analyzed. By analyzing the key parameters affecting the damping effect, the optimal design of the rootless cable damper is studied to provide a foundation for further studies.

2 Simulation model

2.1 Particle damper modeling by the DEM

The discrete element model of a particle damper is based on the conceptual framework proposed by Cundall and Strack [11]. A typical simulation is performed through the following steps.

a) Initialize forces acting on the elements according to the initial conditions or previous step.

b) Detect collisions.

c) Solve interaction functions and apply forces on elements.

d) Change the positions of elements by integrating dynamic equations.

The process is repeated until the simulation is finished.

In the case of a particle damper, each particle is an element. The container is another element with a different material. The total force exerted on the container is the sum of the interaction forces applied by particles in contact with it.

To calculate the interaction forces, a classical Hertz–Mindlin model [14,15] is employed because the parameters are simple with clear physical meanings. Another advantage of this model is that it segregates the normal and tangential forces, which are related to collision and friction, respectively. Rolling friction is considered by applying a constant torque model [16].

In particular, the normal force F_{n} is the sum of the normal contact force F_{cn} and normal damping force F_{dn},

$$F_{\mathrm{n}} = F_{\mathrm{cn}} + F_{\mathrm{dn}}, \tag{1}$$

$$F_{\mathrm{cn}} = \frac{2}{3} k_{\mathrm{n}} \delta_{\mathrm{n}}, \tag{2}$$

$$F_{\mathrm{dn}} = 2\sqrt{\frac{5}{6}} \beta k_{\mathrm{n}}^{0.5} m^{*0.5} \dot{\delta}_{\mathrm{n}}, \tag{3}$$

where δ_{n} is the overlap in the normal direction. k_{n} (normal stiffness), β (damping ratio), and m^* (equivalent mass) are

$$\beta = \frac{\ln e}{\sqrt{\ln^2 e + \pi^2}}, \tag{4}$$

$$k_{\mathrm{n}} = 2E^* \sqrt{R^* \delta_{\mathrm{n}}}, \tag{5}$$

$$m^* = \left(\frac{1}{m_i} + \frac{1}{m_j} \right)^{-1}, \tag{6}$$

where $E^* = \left(\frac{1-v_i^2}{E_i} + \frac{1-v_j^2}{E_j} \right)^{-1}$ (equivalent modulus of the two contact elements), $R^* = \left(\frac{1}{R_i} + \frac{1}{R_j} \right)^{-1}$ (equivalent radius), and e is the coefficient of restitution [17].

The tangential force model is composed of a tangential contact force and tangential damping force,

$$F_{\mathrm{t}} = k_{\mathrm{t}} \delta_{\mathrm{t}} + 2\sqrt{\frac{5}{6}} \beta k_{\mathrm{t}}^{0.5} m^{*0.5} \dot{\delta}_{\mathrm{t}}, \tag{7}$$

where δ_{t} is the overlap in the tangential direction and k_{t} is the tangential stiffness,

$$k_{\mathrm{t}} = 8G^* R^{0.5} \delta_{\mathrm{n}}^{0.5}, \tag{8}$$

where G^* is the equivalent shear modulus,

$$G^* = \left(\frac{1-v_i}{G_i} + \frac{1-v_j}{G_j} \right)^{-1}. \tag{9}$$

The tangential force is limited by the Coulomb friction $\mu_{\mathrm{sf}} F_{\mathrm{cn}}$, where μ_{sf} is the coefficient of sliding friction [11].

The rolling friction is considered by applying a torque to the contacting elements,

$$M_i = \mu_{\mathrm{rf}} F_{\mathrm{cn}} R_i v_i, \tag{10}$$

where μ_{rf} is the coefficient of rolling friction and v_i is the unit angular velocity vector of the contacting element.

Once the forces on each element are obtained, the position of each element can be calculated by integrating the dynamic equation,

$$m_i \frac{\mathrm{d}^2}{\mathrm{d}t^2} u_i = \Sigma F, \tag{11}$$

where m_i and u_i are the mass and position of element i, respectively, and ΣF is the total force exerted on it.

The model in this study was developed using the software EDEM. To further improve the speed of the numerical simulation, the particle damper prototype was simplified. The inside of the container was designed as a single cavity. The thickness of the wall was not considered. The corresponding mass of the container was set directly. The numerical model and its parameters are presented in Fig. 1 and Table 1.

2.2 Cable modeling by the MBD method

A horizontally placed cable was chosen to simulate the

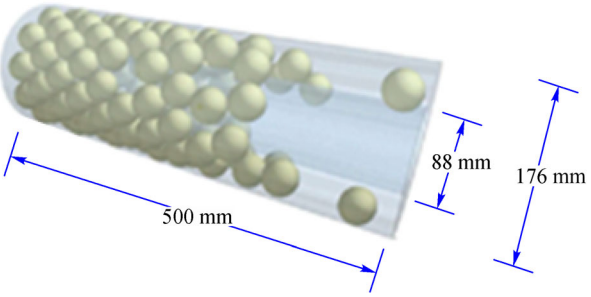

Fig. 1 Numerical model of the damper.

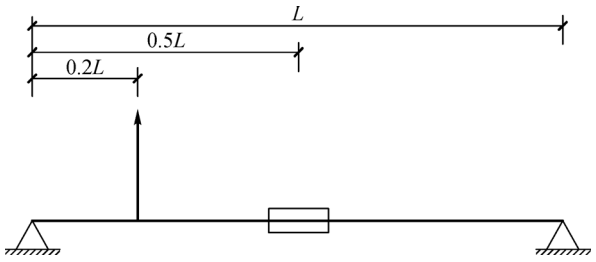

Fig. 2 Cable with the attached damper.

typical vibration phenomenon of cables, as shown in Fig. 2. Both ends are simply supported. A particle damper is installed at the midpoint. The sag effect and bending stiffness of the cable are neglected in the model, as our focus is on the particle parameters. The inner damping of the cable is also ignored. This is acceptable because the inherent damping of cables of cable-stayed bridges is low, usually between 0.1% and 0.15% [18]. The parameters of the cable are listed in Table 2. In the numerical simulations, a sinusoidal excitation is applied at the $0.2L$ point from the end of the cable. The vertical response at the middle point of the cable was calculated.

The model was developed and simulated using the MBD method with the software ADAMS. The cable is composed of a chain of 100 discrete elements; every element has a mass and infinite stiffness. Approximate elements are hinged together in every direction. The connection stiffness is a function of the cable material and geometry. They can be derived according to Ref. [19] and are listed in Table 3. The translational degrees of freedom at the two ends are fixed to simulate simple supports.

The consolidation point on the cable with the particle damper is in the middle, which implies that the force acting on the container is directly applied to the midpoint of the cable. This choice of damper position minimizes the first vibration mode of the cable, which contains most of the energy.

Table 1 Parameters of the damper

object	parameter type	parameter name and unit	value
particle	inherent parameter	density (kg/m^3)	7850
		elastic modulus (MPa)	2×10^5
		Poisson's ratio	0.3
	particle-to-particle contact parameter	coefficient of restitution	0.2
		coefficient of sliding friction	0.5
		coefficient of rolling friction	0.01
container	inherent parameter	elastic modulus (MPa)	2×10^5
		Poisson's ratio	0.3
	particle-to-container contact parameter	coefficient of restitution	0.2
		coefficient of sliding friction	0.5
		coefficient of rolling friction	0.01

Table 2 Geometric and mechanical parameters of the cable model

length (m)	unit mass (kg/m)	cable force (kN)	cross-sectional area (m^2)	elastic modulus (MPa)
100	25.9	3162	6.273×10^{-3}	2×10^5

Table 3 Connection parameters of the cable model

parameter name	direction	value
stiffness coefficient	axial direction (N/mm)	1.3×10^4
	tangential direction (N/mm)	1×10^4
	flexural rigidity (N·mm/rad)	8.46×10^6
tension force	axial direction (N)	3.162×10^6

The first three modes of the cable are crucial because the main requirement of a cable damping system is to provide a sufficient damping to the first three or four cable modes [18]. Thus, verification must be performed to determine whether the cable model generates the required modes.

Various models have been reported for analyses of cable vibrations [20,21]. The classic string theory simplifies the cable into a tensioned string, hinged at both ends. This provides the undamped natural frequency of the cable [22],

$$f_i = \frac{i}{2L}\sqrt{\frac{T}{\varepsilon}}, \tag{12}$$

where i is the frequency order, L is the length, T is the tension in the cable, and ε is the unit mass of the cable.

The results of the modeling of the designed cable in ADAMS are presented in Fig. 3, which shows the first three vibration modes of the cable.

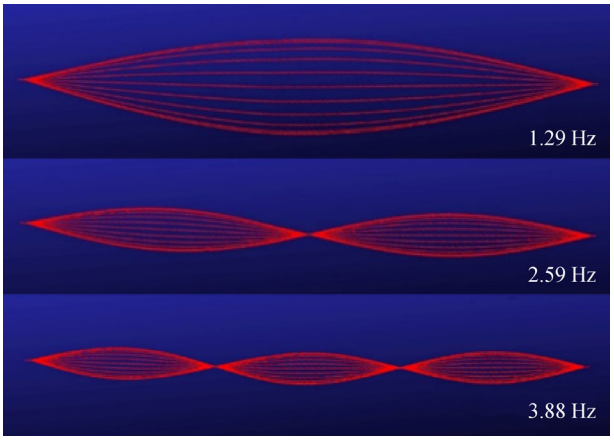

Fig. 3 First three mode shapes of the cable.

The deviations between the first three natural vibration frequencies obtained by the string theory formula and natural vibration frequency of the model are shown in Table 4.

Table 4 First three mode frequencies of the cable

mode	ADAMS model	string theory	deviation
1	1.29	1.24	0.04
2	2.59	2.47	0.05
3	3.88	3.71	0.04

The frequencies calculated by the numerical model match the analytical results, with deviations smaller than 5%. Thus, the model is validated.

During the simulation, in each time step, forces and torques acting on the container calculated by the DEM are transmitted to the cable model at the consolidation point, while displacement data calculated by MBD are returned to the particle damper model. Thus, a cable–damper system model for simulation is established.

3 Results

3.1 Damping performance of the particle damper

The acceleration root mean square value is used to measure the severity of structural vibration,

$$a_{\mathrm{RMS}} = \sqrt{\frac{\sum_{i=1}^{k} a_i^2}{k}}, \tag{13}$$

where a_i is the acceleration at the ith data point and k is the number of data points. In this study, the results for the first 5 s were obtained in each simulation and data were recorded every 10^{-3} s. We define the normalized response η to describe the response of the cable with the particle damper,

$$\eta = \frac{a_{\mathrm{RMS}}^{\mathrm{P}}}{a_{\mathrm{RMS}}}, \tag{14}$$

where $a_{\mathrm{RMS}}^{\mathrm{P}}$ is the root mean square of the acceleration of the structure with the attached particle damper and a_{RMS} is the root mean square of the acceleration of the original structure.

A sinusoidal excitation with a frequency of 1 Hz and amplitude of 18 kN was applied to obtain the time histories of the structures with the particle damper, as shown in Fig. 4(a). The structural vibration is significantly reduced with the particle damper. However, the particle damper causes an additional vibration with a low magnitude and high frequency, possibly owing to the impact forces between the particles and container.

The time effect of the damping was studied by calculating the normalized response at intervals. Considering that the first-order period of the cable is 0.772 s, the calculation interval is set to 0.8 s. Figure 4(b) shows the normalized responses calculated at 0.4, 1.2, 2.0, 2.8, 3.6, and 4.2 s. The particle damper exhibited higher performances in the late stages of vibration than in the initial stage. This indicates that the damping effect of the particle damper has a certain time lag. After the first second, the normalized response decreased to below 0.7 and was 0.40 at 4.2 s, half of the response at 0.4 s.

The excitation frequency was then changed from 1 to 20 Hz to study the effect of the vibration frequency on the damping efficiency. The magnitude of the excitation force was adjusted so that the maximum displacement at the middle point of the cable was always 100 mm. The damper was filled with 100 particles with a radius of 20 mm.

Figure 5(a) shows the normalized response of the cable when the structure was subjected to a sinusoidal excitation with a frequency of 1 to 20 Hz. The particle damper produced a good damping effect in this frequency range. The response decreased with the increase in the excitation frequency. When the excitation frequency was 20 Hz, the

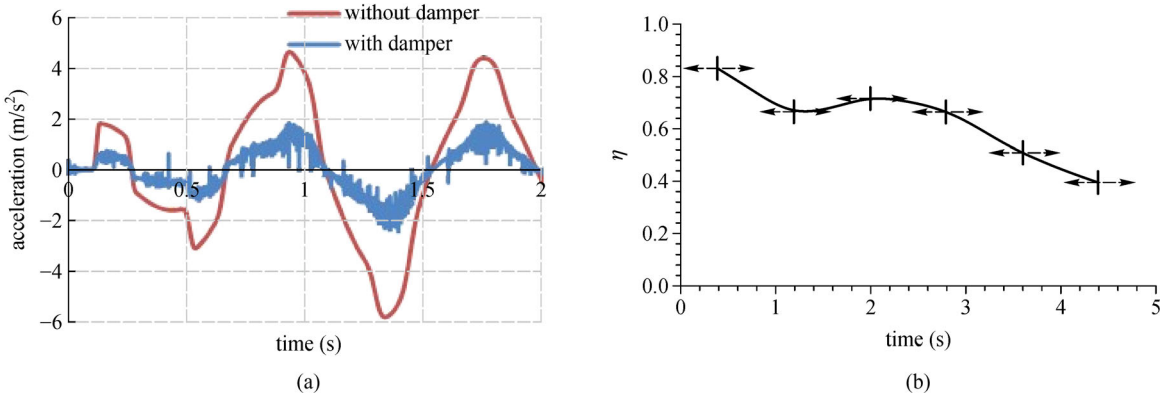

Fig. 4 Damping efficiency of the particle damper. (a) Acceleration time history at the midpoint; (b) time history of the normalized response.

normalized response of the cable with the particle damper was almost half of that without the particle damper.

The influence of the excitation intensity on the performance of the particle damper was also investigated. Excitations with a frequency of 20 Hz and different amplitudes were applied to the cable. The amplitudes at the middle point of the cable were 50, 100, 200, 300, and 500 mm. Figure 5(b) shows the variation of the normalized response at different excitation intensities. In the amplitude range of 50–500 mm, the additional damping from the damper was not considerably changed.

The results show that, for a cable under a sinusoidal excitation, the particle damper produces a good damping effect in a wide frequency range, while the damping efficiency is slightly affected by the vibration intensity.

The numerical simulations of the above cable–damper system show that the use of a particle damper attached to the cable is a feasible solution to suppress the cable vibration. The damper has a considerable damping effect in a wide frequency range. With the increase in the excitation frequency, the damping efficiency tends to increase. However, the particle damper experiences a certain hysteresis to changes in the vibration state, but responds after 1 s and produces a stable damping effect.

3.2 Design parameter analysis

In the previous section, the damping efficiency of the particle damper was studied by applying excitations with different frequencies and intensities to the cable, while the design parameters of the damper were fixed. The damping efficiency of the damper may also change according to its design parameters. In this section, simulations of the damper's efficiency under varying design parameters, including the filling ratio, radius, coefficient of restitution, and coefficient of sliding friction, are presented to determine their influences on the design.

To obtain the maximum number of cycles in a limited simulation time (1 s of simulation equals 4 h of calculation), excitations with a frequency of 20 Hz are used in the parameter analysis. Typical time histories of the displacement and acceleration of the cable are shown in Fig. 6.

3.2.1 Filling ratio

The ratio of the total volume of particles to the volume of the cavity is defined as the filling ratio, expressed as

$$x = \frac{V_{\mathrm{P}}}{V} = \frac{n\pi d^2}{\pi(D_1^2 - D_2^2)H}, \tag{15}$$

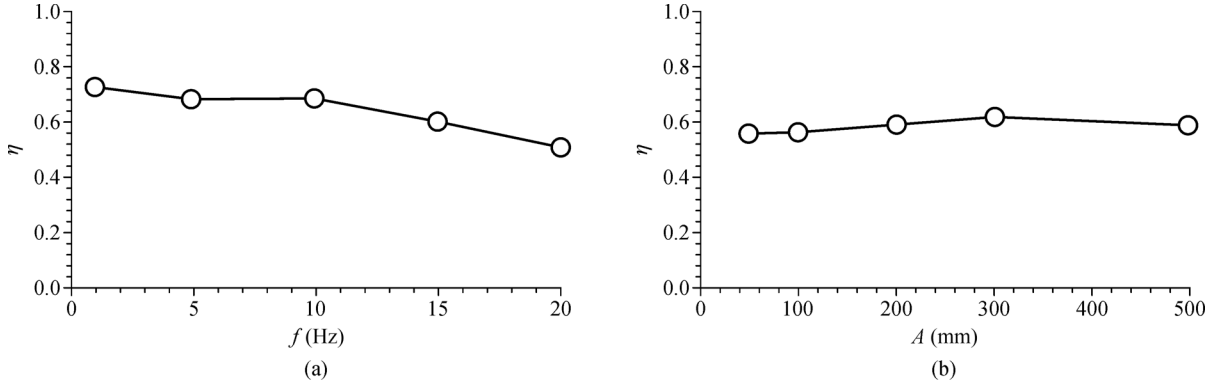

Fig. 5 Normalized responses under different excitations. (a) Influence of the excitation frequency; (b) influence of the excitation intensity.

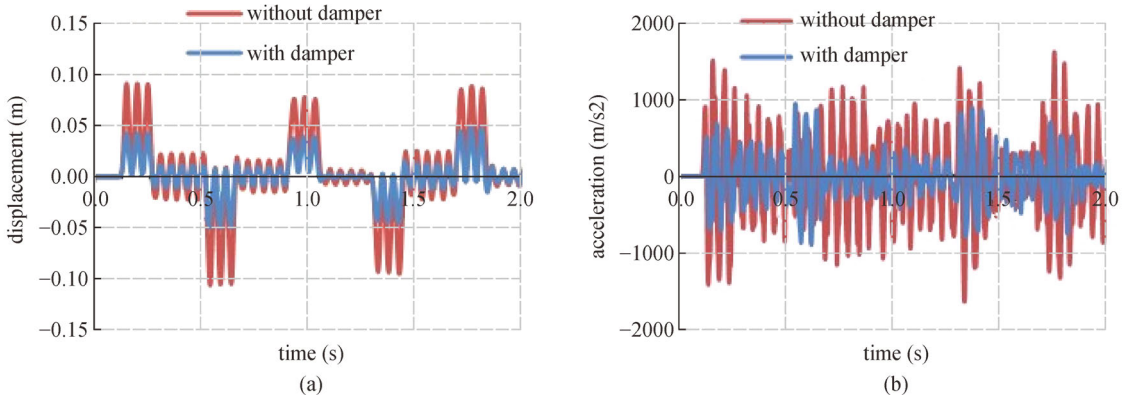

Fig. 6 Typical response of the cable at an excitation frequency of 20 Hz. (a) Displacement; (b) acceleration.

where n is the number of particles, d is the diameter of the particles, V is the volume of the cavity, and D_1 and D_2 are the outer and inner diameters of the damper's cross section, respectively.

The filling ratios were set to 0.073, 0.147, 0.220, 0.294, 0.367, and 0.441 by changing the number of particles. The responses of the structure at an excitation frequency of 20 Hz and excitation amplitude of 100 mm were calculated. Figure 7(a) shows the structural responses for the various filling ratios. Figure 8 shows this series of particle dampers with different filling ratios.

Figure 7(a) shows that the normalized response of the cable initially decreased, and then increased with the filling ratio. The optimal filling ratios are between 0.294 and 0.441. When there were few particles, the possibility of contact between particles and between particles and container wall increased when more particles were placed inside, creating a larger energy dissipation. However, as the number of particles continued to increase, the particles began to accumulate and fewer active particles were involved in the tuning effect. The accumulation also reduced the average velocity of the particles, leading to a

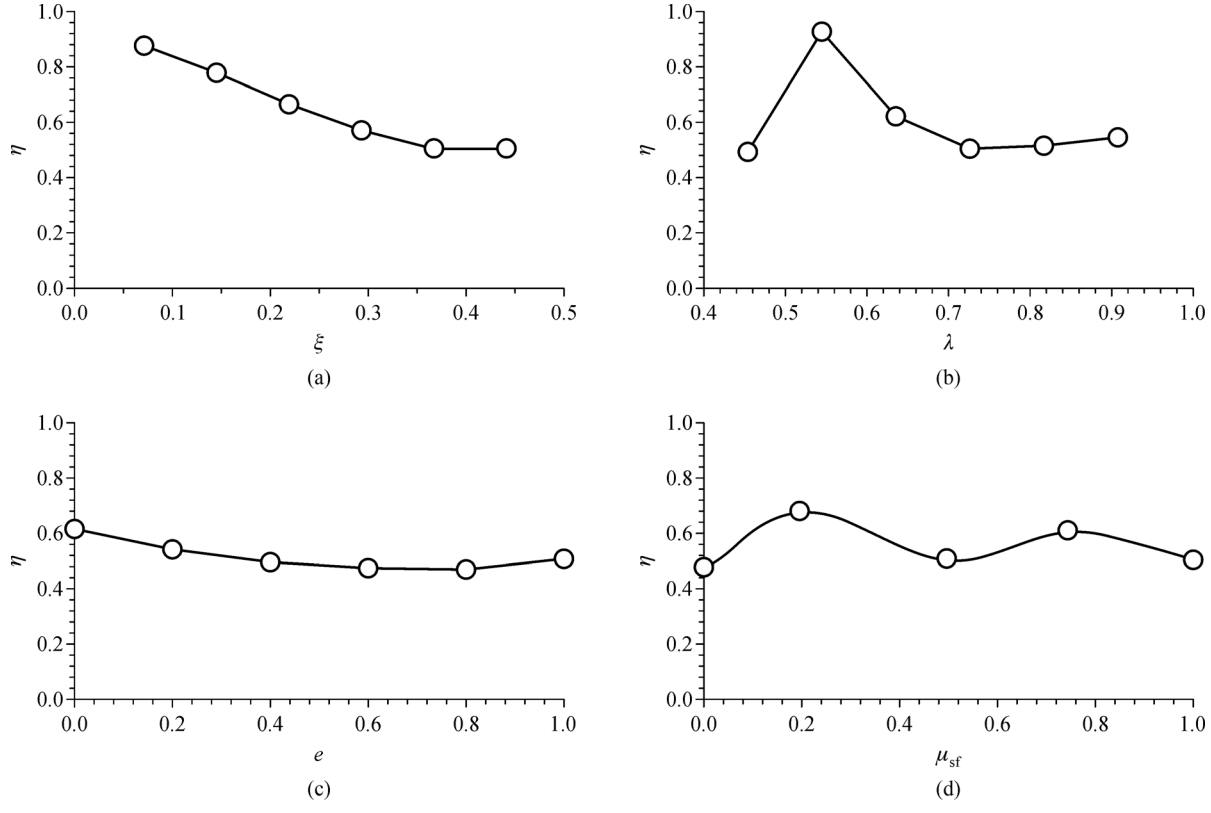

Fig. 7 Influences of the damper's design parameters. (a) Filling ratio; (b) radius of the particles; (c) coefficient of restitution; (d) coefficient of friction.

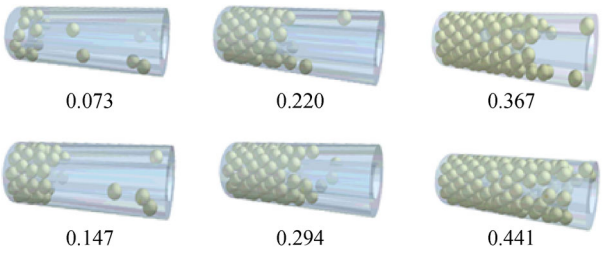

Fig. 8 Particle dampers with different filling ratios.

lower energy dissipation in each contact. Therefore, the damping efficiency was reduced beyond a certain filling ratio.

3.2.2 Radius of the particles

The particle radius is one of the most important parameters in the contact model. A larger particle radius implies a larger damping coefficient in the contact model and larger damping force at the same collision speed (Eq. (3)). However, the stiffness in the contact model is also increased (Eq. (4)). Therefore, the elastic force is larger and the damping force is decreased. In addition, at the same filling ratio, a larger particle radius implies fewer particles and lower probability of particle-to-particle contact. These three effects also exist in the particle-to-wall contact. To transform the particle radius to a dimensionless form, the ratio of the particle radius to the width of the cavity is defined as

$$\lambda = \frac{d}{D_1 - D_2}. \tag{16}$$

The particle size and number of particles were changed simultaneously for a constant filling ratio of 0.367. The effect of the particle size on the performance of the particle damper at the excitation frequency of 20 Hz and excitation amplitude of 100 mm is evaluated. Figure 7(b) shows the changes in the response of the cable at λ of 0.455, 0.545, 0.636, 0.727, 0.818, and 0.909.

When λ was 0.727, 0.818, and 0.909, the normalized responses were 0.7, 0.71, and 0.73, respectively, which implies that, when the filling ratio was constant, smaller particles could achieve a higher damping efficiency. This indicates that, for larger particles, the increase in stiffness coefficient and reduction in contact possibility are more influential than the increase in damping coefficient, causing a lower energy loss. However, this does not imply that a smaller radius implies a better damping. When the particle size ratio λ was 0.636 and 0.545, the normalized response increased sharply, indicating a sharp decrease in the damping effect, because, when the particle diameter is slightly larger than half of the width of the cavity, "clogging" occurs. Figure 9(a) shows a screenshot during the simulation at 1.938 s when $\lambda = 0.545$, where clogging is observed. The minimum particle velocity was 0.01 m/s (blue), while the maximum particle velocity was 1.17 m/s (red). When clogging occurred, most of the particles moved at low speeds and their positions remained unchanged. The energy dissipation of these clogging particles through collision and friction was negligible. The number of effective particles that dissipate energy was considerably smaller than the total number of particles. These immobile particles hindered the movement of moving particles, so that the damping efficiency was largely reduced. When the particle radius continued to decrease to $\lambda = 0.455$, the clogging phenomenon disappeared. As shown in Fig. 9(b), blue represents the minimum particle velocity of 0.05 m/s, while red represents the maximum particle velocity of 2.46 m/s. All particles could move freely in the container and the damping capacity of the damper recovered.

3.2.3 Coefficient of restitution

The coefficient of restitution was used to measure the energy loss during a collision. A smaller value implies more kinetic energy transformed to heat during the collision and lower final velocity after the collision. However, a lower speed implies a mild-motion mode, which is not conducive to frequent collisions among particles and between particles and container.

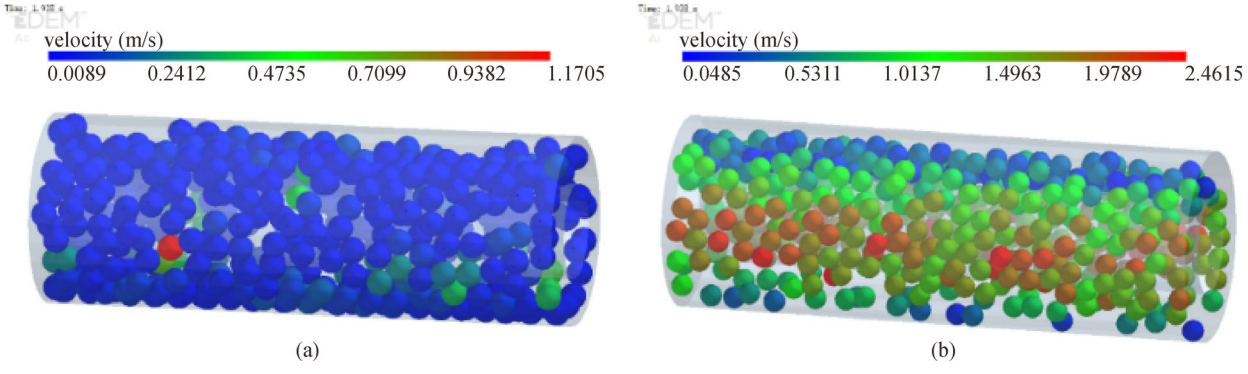

Fig. 9 Screenshots at 1.938 s with different particle radii. (a) The dimensionless radius is 0.545; (b) the dimensionless radius is 0.455.

Figure 7(c) shows the fluctuation in the normalized response for various coefficients of restitution at the particle radius of 20 mm and filling ratio of 0.367.

The damping efficiency initially increased, and then decreased with the increase in the coefficient of restitution. The initial increase occurred because, when the final speed after each collision was larger, the particles moved more violently, stimulating more collisions. Thus, the total collision energy increased and the damping efficiency was improved. However, as the coefficient of restitution continued to increase, the effect of energy dissipation reduction in a single collision exceeded the effect of the increase in collision time. Thus, the total energy dissipation by collisions became smaller and the damping efficiency was reduced. The optimal coefficient of restitution was determined to be approximately 0.8.

3.2.4 Coefficient of friction

For spherical particles, the coefficient of friction controls the maximum tangential force when particles collide. A larger value implies a larger tangential force and more dissipated energy. When the coefficient of sliding friction is 0, no energy dissipation exists in the tangential direction.

Figure 7(d) shows the normalized responses of the cable when the sliding friction coefficients μ_{sf} are 0, 0.2, 0.5, 0.75, and 1.

According to Fig. 7(d), when the coefficient of sliding friction was between 0 and 1, the responses fluctuated between 0.68 and 0.84. When the friction coefficient was 0, the normalized response was smallest and the vibration damping effect was best. This indicates that the tangential energy dissipation does not have a key role in the damping efficiency of a rootless cable damper. Figure 10 shows the relationships between the total energy dissipation, normal energy dissipation, tangential energy dissipation, and coefficient of sliding friction. When the coefficient was 0, the total energy dissipation was largest. The normal energy dissipation corresponded to 100% of the total energy dissipation. With the increase in the coefficient of sliding friction from 0 to 0.5, the tangential energy dissipation increased, while the normal energy dissipation decreased. However, the reduction rate was larger than the increase rate, so that the total energy dissipation continued to decrease. After the coefficient of sliding friction exceeded 0.5, the proportions of normal and tangential energy dissipations tended to be stable, approximately 40% and 60%, respectively. In this case, the total energy dissipation slowly increased. However, even when the coefficient of sliding friction reached the maximum value of 1, the total energy dissipation was not as large as that when the coefficient was 0.

Therefore, with the change in the coefficient of sliding friction, the total energy dissipation reached its maximum when the tangential energy dissipation was completely reduced to zero. The positive effect of this design exceeds the negative effect, which optimizes the damping efficiency of the particle damper.

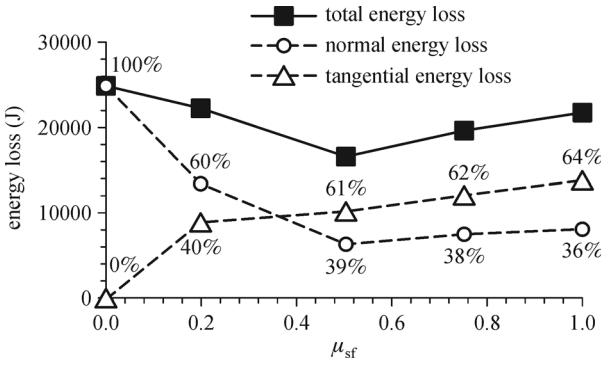

Fig. 10 Influence of the coefficient of sliding friction on the energy loss.

4 Conclusions

In this study, according to the prototype of the rootless cable particle damper [7], a calculation model for the cable–particle damper system was developed. The DEM was used to simulate the particle damper, while the MBD method was used to simulate the cable. The response of the model under a sinusoidal excitation was calculated using the commercial software packages EDEM and ADAMS. The key parameters in the particle damper energy dissipation model were further studied. The influences of the excitation frequency, excitation amplitude, filling ratio, particle size, coefficient of restitution, and coefficient of sliding friction on the damping efficiency through different energy-consuming mechanisms were analyzed. The conclusions of this study can be summarized as follows.

1) The particle damper produced a good damping effect on the cable. The response of the cable could be reduced by 50% in terms of the root mean square of acceleration. However, the impact forces between the particles and container caused additional high-frequency vibrations of the cable.

2) The damping capacity of the particle damper remained high under the simple harmonic excitation in the frequency range of 0–20 Hz and amplitude range of 50–500 mm.

3) When the filling ratio was between 0.294 and 0.441, the damping effect of the cable damper was optimal. A particle damper with a filling ratio higher than 0.441 had a weaker damping effect owing to the crowding of particles.

4) Smaller particles provided a higher damping efficiency than that of larger particles. However, when the particle diameter was slightly larger than half of the width of the cavity, the particles clogged during the vibration and the vibration damping efficiency was sharply reduced.

5) Although a smaller coefficient of restitution led to a higher energy dissipation in a single collision, for a multi-particle damper system, the coefficient of restitution had a different optimal value. A too small value implied a slow particle movement and increased duration of each collision, which led to a reduction in the number of collisions. Thus, the damping efficiency was reduced. The optimal value was 0.8.

6) A larger coefficient of sliding friction led to a larger energy dissipation in the tangential direction and lower in the normal direction. However, when the coefficient of sliding friction was 0, the total energy dissipation was largest and the particle damper provided the highest vibration damping efficiency.

The damping mechanism of the particle damper involved interactions among various parameters. This study considered only the separate influence of a single parameter. In future studies, multi-parameter integration should be considered to complete the parameter analysis and obtain an optimal design.

Acknowledgements This study was supported by the National Natural Science Foundation of China (Grant No. 5187849); National Key R&D Program of China (2017YFF0205605); Shanghai Urban Construction Design Research Institute Project "Bridge Safe Operation Big Data Acquisition Technology and Structure Monitoring System Research"; and Ministry of Transport Construction Science and Technology Project "Medium–Small Span Bridge Structure Network Level Safety Monitoring and Evaluation."

References

1. Abdel-Ghaffar A M, Khalifa M A. Importance of cable vibration in dynamics of cable-stayed bridges. Journal of Engineering Mechanics, 1991, 117(11): 2571–2589
2. Dan D, Ge L, Yan X. Identification of moving loads based on the information fusion of weigh-in-motion system and multiple camera machine vision. Measurement, 2019, 144: 155–166
3. Duan Y F, Ni Y Q, Ko J M. State-derivative feedback control of cable vibration using semiactive magnetorheological dampers. Computer-Aided Civil and Infrastructure Engineering, 2005, 20(6): 431–449
4. Weber F, Boston C. Energy based optimization of viscous–friction dampers on cables. Smart Materials and Structures, 2010, 19(4): 045025
5. Li J, Liu Z, Liu Z, Huang L, Zhou C, Liu X, Zhu W. Electromechanical characteristics and numerical simulation of a new smaller magnetorheological fluid damper. Mechanics Research Communications, 2018, 92: 81–86
6. Pacheco B M, Fujino Y, Sulekh A. Estimation curve for modal damping in stay cables with viscous damper. Journal of Structural Engineering, 1993, 119(6): 1961–1979
7. Dan D, Gong J, Chen Z, Sun L. CN Patent, CN10316-1124A, 2013-06-19
8. Luo Z, Yan W, Xu W, Zheng Q, Wang B. Experimental research on the multilayer compartmental particle damper and its application methods on long-period bridge structures. Frontiers of Structural and Civil Engineering, 2019, 13(4): 751–766
9. Wu W T, Aubry N, Massoudi M. Flow of granular materials modeled as a non-linear fluid. Mechanics Research Communications, 2013, 52: 62–68
10. Lu Z, Lu X, Jiang H, F. Masri S. Discrete element method simulation and experimental validation of particle damper system. Engineering Computations, 2014, 31(4): 810–823
11. Cundall P A, Strack O D L. A discrete numerical model for granular assemblies. Geotechnique, 1979, 29(1): 47–65
12. Ahmad N, Ranganath R, Ghosal A. Modeling and experimental study of a honeycomb beam filled with damping particles. Journal of Sound and Vibration, 2017, 391: 20–34
13. Hou Y, Wang L. Multiscale mechanical modeling of hydrated cement paste under tensile load using the combined DEM-MD method. Frontiers of Structural and Civil Engineering, 2017, 11(3): 270–278
14. Zhou Y C, Wright B D, Yang R Y, Xu B H, Yu A B. Rolling friction in the dynamic simulation of sandpile formation. Physica A, 1999, 269(2–4): 536–553
15. Mindlin R D, Deresiewicz H. Elastic spheres in contact under varying oblique forces. Journal of Applied Mechanics, 1953, 9: 327–344
16. Sakaguchi H, Ozaki E, Igarashi T. Plugging of the flow of granular materials during the discharge from a silo. International Journal of Modern Physics B, 1993, 7: 1949–1963
17. Tsuji Y, Tanaka T, Ishida T. Lagrangian numerical simulation of plug flow of cohesionless particles in a horizontal pipe. Powder Technology, 1992, 71(3): 239–250
18. Weber F, Distl H. Amplitude and frequency independent cable damping of Sutong Bridge and Russky Bridge by magnetorheological dampers. Structural Control and Health Monitoring, 2015, 22(2): 237–254
19. Mcisaac K A. A hierarchical approach to motion planning with applications to an underwater eel-like robot. Dissertation for the Doctoral Degree. Philadelphia, PA: University of Pennsylvania, 2001
20. Dan D, Han F, Cheng W, Xu B. Unified modal analysis of complex cable systems via extended dynamic stiffness method and enhanced computation. Structural Control and Health Monitoring, 2019, 26(10): e2435
21. Han F, Dan D, Cheng W, Zang J. A novel analysis method for damping characteristic of a type of double-beam systems with viscoelastic layer. Applied Mathematical Modelling, 2020, 80: 911–928
22. Hoang N, Fujino Y. Multi-mode control performance of nonlinear dampers in stay cable vibrations. Structural Control and Health Monitoring: The Official Journal of the International Association for Structural Control and Monitoring and of the European Association for the Control of Structures, 2009, 16(7–8): 860–868